JOURNAL OF GEOPHYSICAL RESEARCH, VOL. 112, D22S10, doi:10.1029/2006JD008337, 2007

Estimation of aerosol effects on surface irradiance based on measurements and radiative transfer model simulations in northern China

X. Xia,[1] Z. Li,[2] P. Wang,[1] H. Chen,[1] and M. Cribb[2]

Received 11 December 2006; revised 6 April 2007; accepted 17 July 2007; published 31 August 2007.

[1] Using 15 months' worth of ground-based broadband and spectral radiation data at Xianghe, a suburban site in northern China, aerosol effects on surface irradiance are explored in this study. Collocated aerosol optical depth (AOD) and surface irradiance measurements made under cloudless sky conditions are first binned according to solar zenith angle. Empirical equations are then developed to describe the relationships between AOD and surface shortwave radiation (SWR) and photosynthetically active radiation (PAR). The equations are finally used to derive quantitative estimates of aerosol effects on surface SWR and PAR. The annual mean aerosol direct radiative forcing (ADRF) values for SWR and PAR derived from measurements are -32.8 and -16.6 W m^{-2}, respectively, which are in good agreement with those derived from radiative transfer model simulations. Variations in aerosol concentration not only change the amount of global solar radiation reaching the Earth's surface but also alter the relative proportions of diffuse and direct solar radiation. The annual mean changes in direct and diffuse SWR induced by aerosols are -89.6 and 51.0 W m^{-2}, respectively, and the annual mean changes in direct and diffuse PAR induced by aerosols are -51.0 and 29.6 W m^{-2}, respectively. The effects of regional haze in China on climate and crop production should be further studied.

Citation: Xia, X., Z. Li, P. Wang, H. Chen, and M. Cribb (2007), Estimation of aerosol effects on surface irradiance based on measurements and radiative transfer model simulations in northern China, *J. Geophys. Res.*, *112*, D22S10, doi:10.1029/2006JD008337.

1. Introduction

[2] It is widely recognized that aerosols directly influence the Earth's radiative balance by backscattering and absorption of shortwave (solar) radiation and indirectly by influencing cloud properties and lifetimes [*Charlson et al.*, 1992]. Over land and from an integration of satellite retrievals and model simulations, aerosol direct radiative forcing (ADRF) has been estimated as equal to -4.9 ± 0.7 W m^{-2} and -11.8 ± 1.9 W m^{-2} at the top of the atmosphere and at the surface, respectively. These are generally larger than estimates by chemical transport model simulations by about 30–40%, even after accounting for thin cirrus and cloud contamination on satellite measurements [*Yu et al.*, 2006]. Because of the relatively short lifetime of aerosol particles and their large regional variability, instances of strong localized direct forcing were revealed from satellite retrievals. Aerosols may cool or warm the climate system depending on aerosol absorption properties and surface albedo, but there is no doubt that aerosols may induce a substantial decrease in surface irradiance via its scattering and absorption of sunlight. *Satheesh and Ramanathan* [2000] pointed out that the aerosol forcing at the top of the atmosphere was only about one-third as great as that at the surface. The difference goes into heating the atmosphere and this heating may affect the water cycle through its effect on local vertical circulations and large-scale monsoon circulations [*Ramanathan et al.*, 2001a].

[3] As one of the largest developing countries, China has experienced rapid economic growth and population expansion, which has lead to an increase in aerosol optical depth (AOD), especially in eastern China where anthropogenic activities result in high aerosol loading all year round [*Luo et al.*, 2001; *Zong et al.*, 2005]. The increase in aerosol loading likely partly accounts for the notable decrease in sunshine duration and surface irradiance [*Che et al.*, 2005; *Liang and Xia*, 2005; *Qian et al.*, 2006]. Regional changes in temperature and precipitation pattern since the mid-1970s in China are probably related to heavy aerosol loading and strong absorption by aerosols [*Li et al.*, 1995; *Xu*, 2001]. Researches on aerosol properties and radiative effects were performed in China and substantial progress was made in recent years [*Wang et al.*, 2001]. The spatiotemporal variations of aerosol optical properties were explored using the ground-based and satellite data [*Li et al.*, 2003; *Xia et al.*,

[1] Institute of Atmospheric Physics, Chinese Academy of Sciences, Beijing, China.
[2] Department of Atmospheric and Oceanic Science and Earth System Science Interdisciplinary Center, University of Maryland, College Park, Maryland, USA.

0148-0227/07/2006JD008337$09.00

2005; *Eck et al.*, 2005; *Xia et al.*, 2006]. The dust radiative forcing was simulated using a dust optical model [*Wang et al.*, 2004] and observed from the ground-based data [*Cheng et al.*, 2006]. Note that the spatial and temporal variations of the complex aerosols throughout the vast territory of China and their effects on climate are still not well known [*Mao and Li*, 2005]; therefore long-term measurements of aerosol loading and aerosol effects on surface irradiance made in the continental source regions of China are still urgently required [*Li*, 2004].

[4] In order to gain insight about aerosol properties and their climatic and environmental effects over this major aerosol source region, a project titled the "East Asian Study of Tropospheric Aerosols: an International Regional Experiment" (EAST-AIRE) commenced in 2004 [*Li et al.*, 2007]. An important goal of the project is to establish 4–5 supersites in China, instrumented with spectral and broadband radiometers, so that multiyear measurements can be made. The ground-based radiation data can be used with satellite data to assess comprehensively aerosol effects on the energy budget in the region.

[5] In September 2004, the first supersite was established at Xianghe, where a set of solar radiometers was installed. More than two year's worth of continuous measurements has been collected so far, which provides an opportunity to examine aerosol effects on surface irradiance. The objective of this study is to estimate aerosol effects on surface shortwave radiation (SWR), photosynthetically active radiation (PAR) and the partitioning of direct and diffuse components. While some of *Li et al.* [2007] are also concerned with aerosol radiative effects, this study differs in several ways. First, the method of estimating the aerosol radiative effect is different. Second, this study includes an analysis of the PAR data. Third, the partitioning of direct and diffuse radiation is studied. Fourth, closure tests are performed which involves comparing measurements with model simulations.

2. Site Description and Instrumentation

[6] In September 2004, a radiation site was established in Xianghe County (39.753°N, 116.961°E, 30 m asl), a suburban region in northern China. The site is located about 80 km southeast of central Beijing. A CIMEL Sun/sky radiometer and a set of broadband radiometers were installed side by side. A Total Sky Imager (TSI) was employed to take snapshots of the overhead sky every minute during the daytime. The instruments were installed on the roof of a four-story building where the field of view is unobstructed in all directions. Radiation data from October 2004 to December 2005 were used in the analysis.

2.1. AERONET Data

[7] A CIMEL Sun/sky radiometer was installed in September 2004 and since then, Xianghe has become one of the Aerosol Robotic Network (AERONET) sites [*Holben et al.*, 1998]. AODs at seven wavelengths (340, 380, 440, 500, 670, 870, and 1020 nm) are retrieved with an uncertainty of $0.01 \sim 0.02$ [*Eck et al.*, 1999]. The measurements at 940 nm are used for the derivation of the water vapor column amount. Aerosol size distribution, refractive index and single-scattering albedo are retrieved from the sky radiance measurements and AODs [*Dubovik et al.*, 2000]. The data presented here are level 2.0 quality-assured data and have been prefield and postfield calibrated, automatically cloud screened [*Smirnov et al.*, 2000] and manually inspected.

Table 1. Broadband Radiometers Used at the Xianghe Site

	Global	Direct	Diffuse	PAR
Instrument	CM21/CM11	NIP	Black&White	PAR-LITE
Wavelength, nm	305–2800	285–2800	285–2800	400–700
Manufacturer	Kipp-Zonen	Eppley	Eppley	Kipp-Zonen

2.2. Broadband Solar Radiation Data

[8] Surface irradiance is measured by a set of solar radiometers (see Table 1). The radiometers take samples every second but 1-min means and standard deviations are saved to a Campbell data logger. Kipp-Zonen CM21 and CM11 radiometers are used to measure global SWR. Global SWR can also be derived by summing the direct and diffuse components of radiation, which are measured separately by an Eppley Normal Incidence Pyrheliometer (NIP) and a black-and-white radiometer (B&W), both mounted on an EKO STR-22 solar tracker. A redundant set of broadband radiometers is used to ensure the precision of measurements, and to rule out possible biases due to physical problems (e.g., misaligned solar shadowing disk). A PAR-LITE quantum sensor is used to measure the photon number density. The radiometers were factory calibrated immediately before installation and ventilated as recommended by the World Climate Research Program's Baseline Surface Radiation Network (BSRN). Radiometer dome cleaning and level checks are performed daily to ensure data quality and consistency. The data are stored at the site and transferred to the University of Maryland overnight where they are visually inspected for quality assurance. Thermopile-based single black detector broadband radiometers are known to suffer from infrared loss from the detector [*Dutton et al.*, 2001; *Philipona*, 2002, *Michalsky et al.*, 2005]. The mean nighttime offsets of the CM21 and CM11 radiometers used in this study, an indicator of the magnitude of the infrared loss in the global measurements, are about -2 W m^{-2} and -4 W m^{-2}, respectively. The nonideal angular response of the CM21 and CM11 radiometers also limits their accuracy to about 3% [*Michalsky et al.*, 1999]. Given these limitations, global SWR was calculated by summing the direct beam radiation measured by the NIP (multiplied by cosine of the solar zenith angle) and the diffuse horizontal radiation measured by the B&W. The data were quality-checked using the Baseline Surface Radiation Network (BSRN) quality control procedure [*Ohmura et al.*, 1998]. The quality-controlled data are then submitted to the Baseline Surface Radiation Network (BSRN) for archiving. The field measurement uncertainties were estimated to be 3%, 6%, and 6% for direct, diffuse and global measurements using NIP and B&W radiometers [*Stoffel*, 2005]. Because the NIP and the shaded and ventilated B&W were used in this study, the measurement uncertainties here should be close to those estimates.

2.3. Total Sky Imager (TSI) Data

[9] A TSI-440 was installed to take pictures of the overhead sky every minute during the daytime. The TSI-440

model is a full-color sky camera with a software package that operates the instrument and performs some data processing functions. A rudimentary estimate of the cloud fraction can be retrieved from an algorithm provided by the manufacturer.

3. Clear-Sky Discrimination From Radiation Data

[10] Because of the focus on aerosol radiative effects under clear-sky conditions, the first step in the analysis is to detect cloud-free skies. This is achieved using an empirical clear-sky detection algorithm proposed by *Long and Ackerman* [2000], with some modifications to better cope with the specific conditions under study. The method is briefly introduced here for completeness.

[11] The global SWR under clear skies can be simulated by a power law function of the cosine of the solar zenith angle (θ) [*Long and Ackerman*, 2000], i.e., $F_{global} = a \times \mu^b$, where F_{global} is the global SWR, μ is the cosine of θ, a and b are two parameters. The value of b is set to 1.2 and the coefficient a is increased gradually to simulate global SWR for clear skies with different aerosol loadings. If 80% of the measurements are less than the computed values given by equation (1) with the specified coefficients, the process is terminated and the corresponding coefficient a is saved. Measurements are probably influenced by cloud if the absolute relative deviation of measurements from the corresponding computed values is greater than 20%. The second test involves normalizing the CM21 measurements by the computed values from equation (1). A running standard deviation over a 30-min period is calculated to check the variability of the normalized radiation. The measurement is deemed affected by cloud if the standard deviation is greater than 0.02. The third test checks whether the B&W measurements are greater than a limit for the maximum diffuse radiation where $Dif_{max} = 350 \times \mu^{0.5}$. Note that Dif_{max} is a factor of 2 larger than that used by *Long and Ackerman* [2000]. This is mostly due to heavy aerosol loading at the Xianghe site and the objective of using 350 W m^{-2} is to retain data points under hazy but cloud-free skies. The presence of clouds can result in a dramatic fluctuation of solar radiation on a short timescale, for example, over a 1-min period, so the fourth test checks the standard deviation of 1-min global (CM21) and B&W data. The data are eliminated if the standard deviations are larger than 0.02. If sufficient clear-sky measurements are identified on a given day, the power law equation is fit to the data [*Long and Ackerman*, 2000] and the cloud-screening method was then performed using new parameters.

[12] Data are identified as measurements under cloud-free skies if they pass the four tests described above. As a final step, the clear-sky radiation data are collocated with AERONET data.

4. Comparison Between Measurements and Model Simulations

[13] The Santa Barbara DISORT Atmospheric Radiative Transfer model (SBDART) was used to estimate surface irradiance. SBDART relies on the LOWTRAN-7 atmospheric transmission data and the radiative transfer equation is numerically integrated with the DISORT radiative transfer module [*Ricchiazzi et al.*, 1998]. SBDART was run with 33 altitude layers and used four radiation streams. SBDART agreed to better than 3% in the broadband calculations of irradiance with measurements [*Halthore et al.*, 2005]. Radiosonde data taken 50 km north of Xianghe are used to describe the vertical profile of the atmosphere. The column-integrated ozone and water vapor amounts are scaled by ozone data from TOMS http://toms.gsfc.nasa.gov) and water vapor data from AERONET. The aerosol inputs to the SBDART model include aerosol optical depth, single-scattering albedo and asymmetry factor at four AERONET wavelengths, i.e., 440, 670, 870 and 1020 nm, which are used to interpolate and extrapolate data into the spectral divisions of the SBDART model. The model interpolates AOD between four wavelengths using the Ångstrom expression and assumes a λ^{-1} AOD dependence outside the aerosol wavelength range using the 440 and 1020 nm end points as anchors. Surface albedo data at seven wavelengths from the Moderate Resolution Imaging Spectroradiometer (MODIS) are used in the simulations [*Schaaf et al.*, 2002]. Figure 1 presents the intercomparison of calculated and measured values. The results show that the model simulations can account for more than 98% of the measurement variances. The mean bias errors (MBE) between mean simulations and mean measurements are 7.9 W m^{-2}; -1.7 W m^{-2}, 6.2 W m^{-2} and -3.0 W m^{-2} for direct (NIP), diffuse (B&W), global (NIP + B&W) and PAR (PAR-LITE), respectively. The MBE values are much less than the root mean square errors (RMSE) and are within model and measurement uncertainties.

[14] As introduced in section 2, the PAR-LITE measures the photon number density, which is a parameter commonly used in ecology. However, the atmospheric science community describes visible radiation using energy units. It was suggested that a constant factor (e.g., 4.57 [*Ross and Sulev*, 2000]) could be used to convert the photon number density to radiative energy under clear-sky conditions. Here, both quantities are calculated by the SBDART and the ratios between them are used to convert individual measurements of photon number density to radiative energy. As a result, PAR presented hereafter has units of W m^{-2} rather than μmol m^{-2} s^{-1}. The model simulations show that the mean ratio and standard deviation are 4.58 and ±0.01, respectively. The ratio increases significantly with AOD and weakly depends on the solar zenith angle (not shown).

5. Aerosol Induced Instantaneous Changes in Surface Radiation

[15] High aerosol loading in Xianghe prevails all year round and the yearly mean AOD is equal to 0.82 [*Li et al.*, 2007]. As a result, aerosols are expected to seriously impact surface irradiance and also the partitioning between the direct and diffuse components of the surface irradiance. The instantaneous changes in the surface irradiance due to aerosol scattering and absorption are presented in this section.

[16] Water vapor is an important atmospheric constituent involved in the absorption of solar radiation and it has a distinct seasonal pattern in northern China. Water vapor effects on the relationship of AOD and surface irradiance

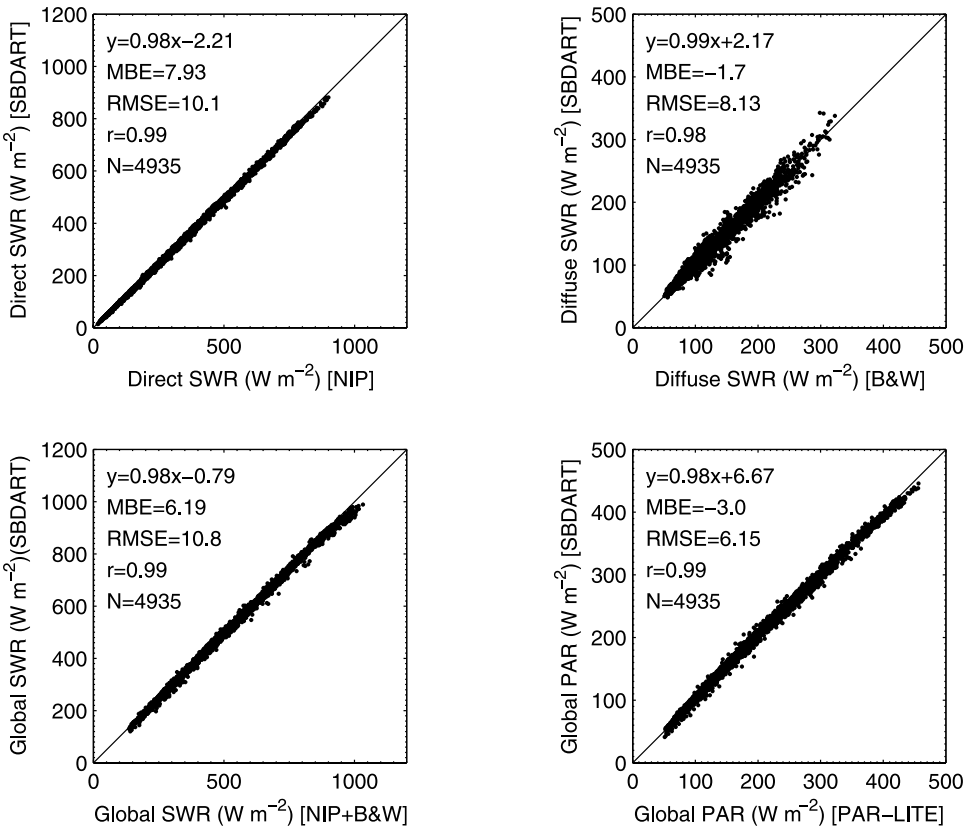

Figure 1. Comparison of surface irradiance measured by radiometers and simulated by the Santa Barbara DISORT Atmospheric Radiative Transfer model (SBDART). The solid black lines represent the 1:1 relation. Also included in the figure are the linear fit equations, the mean bias errors (MBE: mean simulations minus mean measurements), root mean square errors (RMSE) and correlation coefficients (r).

should be considered if data from different months are mixed together [*Li and Trishchenko*, 2001]. Water vapor effects are minimized using the following equation, the function of which is to scale real measurements (with varying water vapor contents) into values with fixed water vapor content through SBDART simulations:

$$F(\theta)_{scaled} = \left[F(\theta)^{fixed}_{SBDART} / F(\theta)^{obs}_{SBDART}\right] \times F(\theta)_{obs} \qquad (1)$$

where $F(\theta)^{fixed}_{SBDART}$ and $F(\theta)^{obs}_{SBDART}$ represent SBDART simulations of surface irradiance using fixed (water vapor corresponding to the maximum occurrence frequency) and measured water vapor contents, respectively.

[17] Since the magnitude of surface irradiance and the spectral distribution depend significantly on the θ, the effects of aerosol on SWR and PAR are analyzed separately for narrow θ ranges. The analysis includes not only changes in global SWR and PAR, but also changes in the partitioning between the direct and diffuse components of the surface irradiance. It is believed that regional haze in China is currently reducing the optimal yields of 70% of the crops grown in China by at least 5–30% because haze induces a 5–30% reduction in global SWR [*Chameides et al.*, 1999]. Note that the benefit of the increase in diffuse SWR due to aerosols for crop growth was not considered. It is believed that a high proportion of diffuse radiation increases the radiation use efficiency of photosynthesis because diffuse radiation is distributed more uniformly over and within leaf surfaces and is able to better penetrate vegetative layers. However, with direct radiation the vegetative sublayers are shaded and the illuminated parts may be light saturated and potentially photoinhibited, possibly resulting in decreased radiation use efficiency [*Roderick et al.*, 2001]. It is useful to determine how much direct radiation is transformed into diffuse radiation via aerosol scattering and how these changes in the partitioning impact crop yield and carbon cycling.

[18] Scatterplots of measured surface global SWR and its direct and diffuse components as a function of AOD for nine θ ranges are shown in Figures 2–4. Relationships between global, direct, diffuse PAR and AOD are also derived, but from PAR-LITE measurements (Figure 5) and SBDART simulations (not shown). The general picture is that direct radiation decreases significantly because of aerosol scattering and absorption, some part of which is offset by a moderate increase in diffuse radiation. Therefore the overall effect of aerosols is to induce a notable reduction in global radiation. Surface irradiance changes linearly with AOD when AOD is less than 0.5, but a nonlinear function is more suitable for the overall relationships. The following exponential equation is used to fit global and direct radiation to AOD:

$$F(\theta) = F_0(\theta) \times \exp[b(\theta) \times AOD] \qquad (2)$$

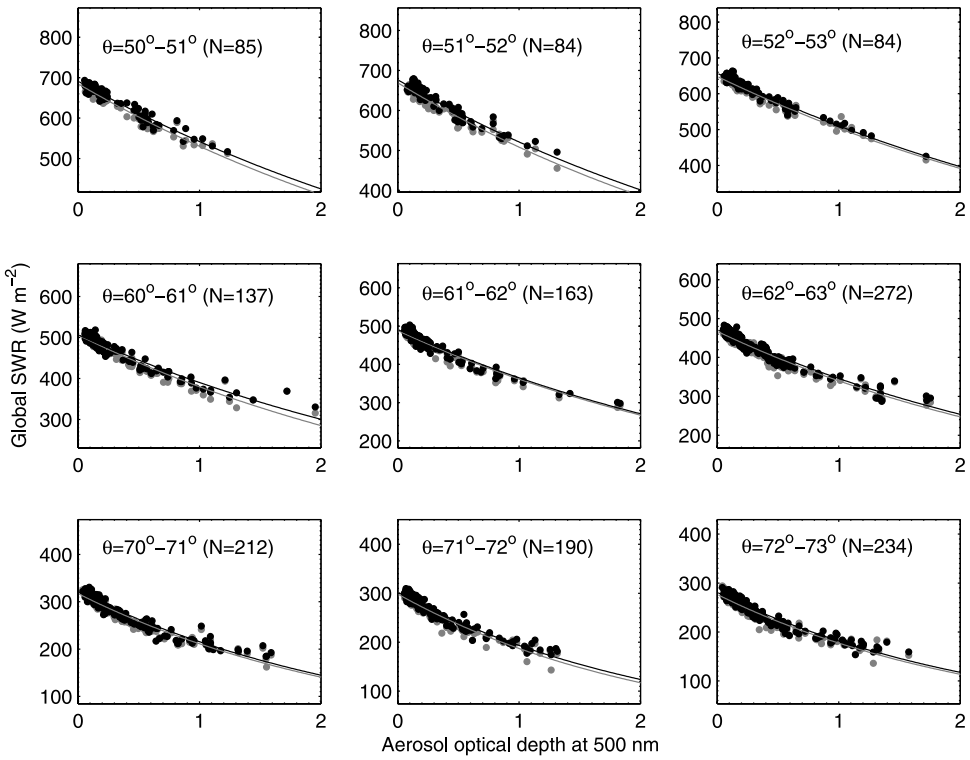

Figure 2. Scatterplots of the global shortwave irradiance as a function of the aerosol optical depth at 500 nm for nine solar zenith angles. Measurements and model simulations are represented by shaded and solid dots, respectively. The shaded and solid lines represent the fitting results using an exponential equation for the measurements and model simulations, respectively.

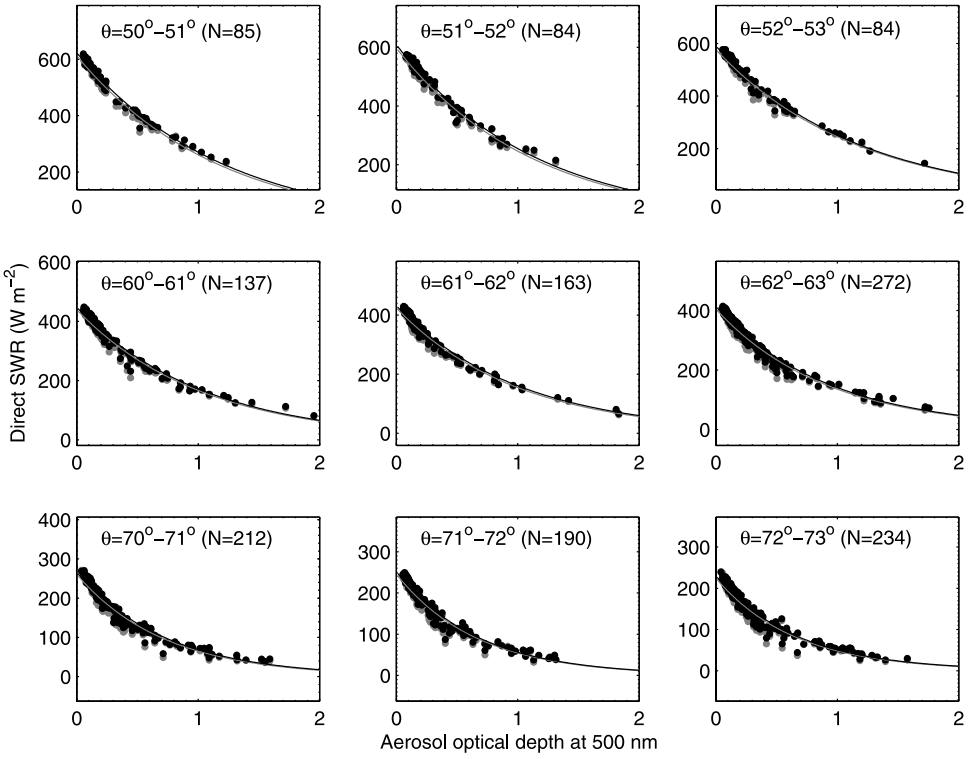

Figure 3. Same as Figure 2 but for direct shortwave irradiance.

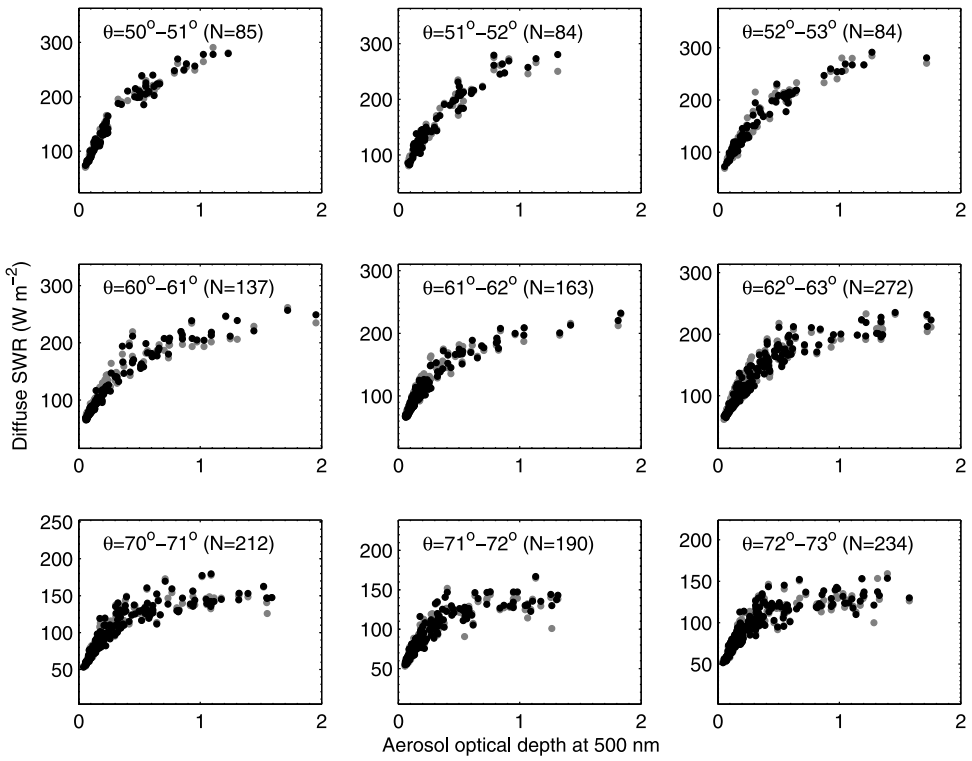

Figure 4. Scatterplots of diffuse shortwave irradiance as a function of the aerosol optical depth at 500 nm for nine solar zenith angles. Measurements and model simulations are represented by shaded and solid dots, respectively.

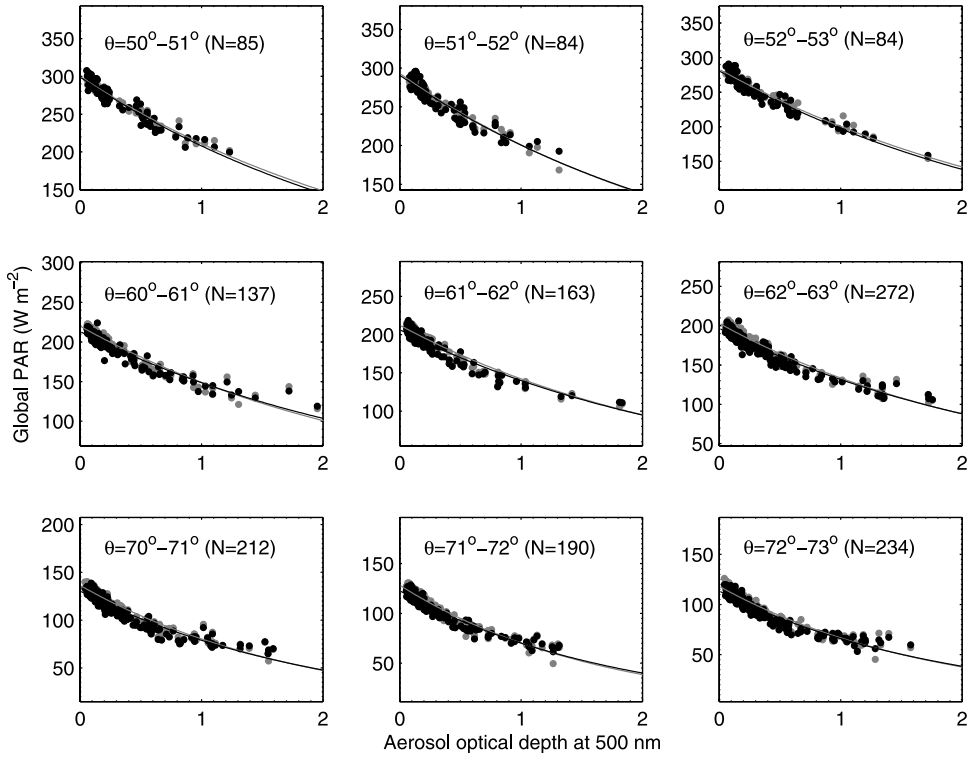

Figure 5. Same as Figure 2 but for global photosynthetically active radiation.

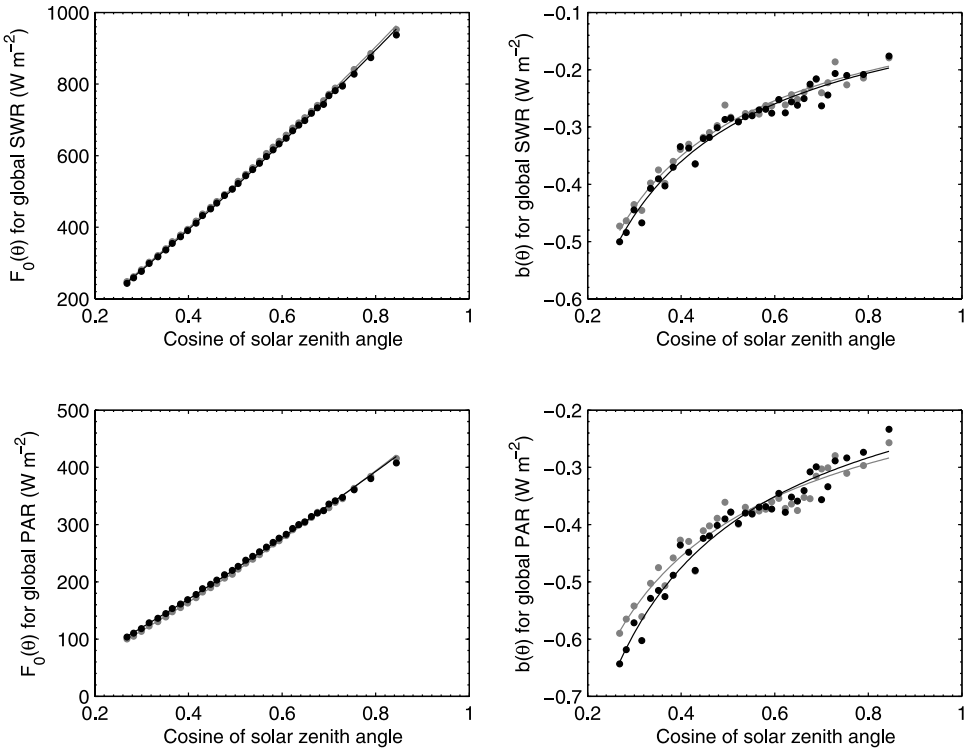

Figure 6. Scatterplots of parameters $F_0(\theta)$ and $b(\theta)$ as a function of the cosine of the solar zenith angle for (top) global shortwave irradiance and (bottom) global PAR.

where $F_0(\theta)$ and $b(\theta)$ are fitting parameters. Note that measurements (represented by gray dots) and model simulations (represented by black dots) are simultaneously plotted in the figures. The correlation coefficients generally exceed 0.90 and reach 0.98 in some cases. The regression analysis shows that the fitting parameters using the two data sets are very close to each other. Note that the first term on the right-hand side of the equation represents the expected surface irradiance when AOD is zero. The second term determines the aerosol effect on atmospheric transmission at a specified θ and AOD. $F_0(\theta)$ is expected to decrease with θ because of decreasing incident sunlight and $b(\theta)$ should decrease moderately with θ because of the increasing atmospheric optical path with θ. Figure 6 presents the scatterplots of $F_0(\theta)$ as a function of μ (Figure 6, left) and $b(\theta)$ as a function of μ (Figure 6, right) for global SWR and PAR. Scatterplots for direct SWR and PAR are shown in Figure 7. The data points can be fit by a linear equation [*Chou et al.*, 2006], but a power law equation is chosen here because it can produce reasonable results when θ is 0° or 90°, i.e., $F(\theta) = a_1 \times \mu^{a_2}$ and $b(\theta) = a_3 \times \mu^{a_4}$. The four parameters are derived using the least squares technique. Instantaneous global and direct irradiance at the surface can then be parameterized as a function of μ and AOD in the following way:

$$F(\theta) = a_1 \times \mu^{a_2} \times \exp[a_3 \times \mu^{a_4} \times AOD] \tag{3}$$

[19] The instantaneous changes in global and direct radiation due to aerosols can be computed as the difference between $F(\theta)$ and $F_0(\theta)$. The change in the diffuse irradiance can then be calculated as the difference between the changes in global and direct irradiance. The instantaneous aerosol direct forcing, i.e., the difference in net global SWR (or PAR), with and without aerosol, can be computed as follows:

$$ADRF_{\text{int}} = (1 - \alpha) \times (F(\theta) - F_0(\theta)) \tag{4}$$

where $ADRF_{int}$ means instantaneous aerosol direct radiative forcing and α represents surface albedo.

6. Diurnal Mean Aerosol Direct Radiative Forcing

[20] Note that the instantaneous effects of aerosols on surface irradiance depend heavily on θ. In order to remove this dependence so that the AOD dependence can be isolated, the diurnal mean aerosol forcing is computed to better represent aerosol climatic and environmental effects. Obtaining a value for the diurnal mean aerosol radiative effect is not straightforward because the passage of clouds frequently interrupts clear-sky data. The conventional method uses a radiative transfer model to extrapolate instantaneous measurements and then derives the diurnal mean aerosol effect [*Conant*, 2000; *Li and Trishchenko*, 2001]. Another method was proposed by *Li et al.* [2007] where clear-sky irradiances were fit as a linear function of θ over whatever time period and then integrated to determine the daily mean ADRF. In general, this method works well unless aerosol properties change dramatically.

[21] Because aerosol-induced instantaneous changes in surface irradiance were parameterized as a function of μ and AOD, the diurnal mean aerosol effect on surface radiation can be derived by integration of these instanta-

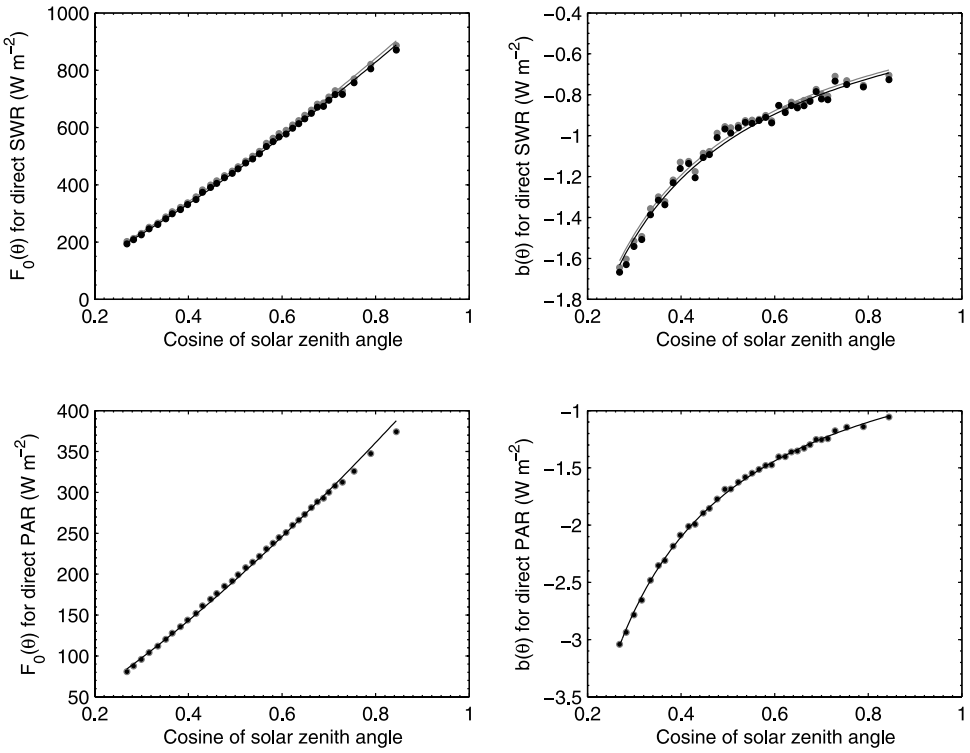

Figure 7. Same as Figure 6 but for (top) direct shortwave irradiance and (bottom) direct PAR.

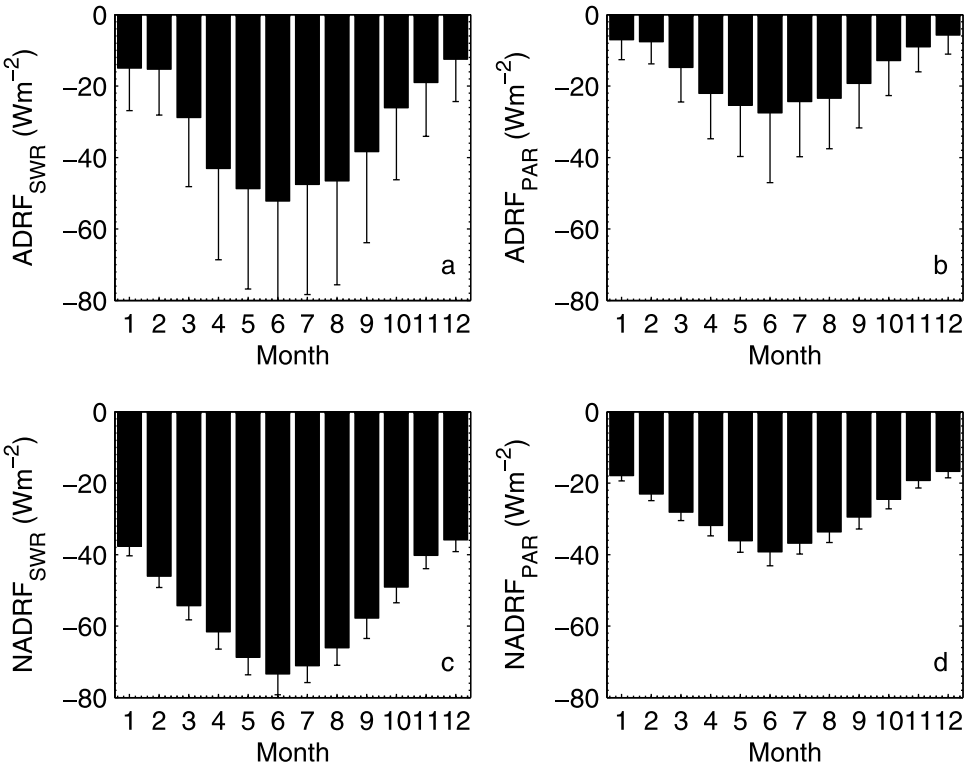

Figure 8. Monthly diurnal mean aerosol direct radiative forcing at the surface (ADRF) and corresponding ADRF per unit AOD (NADRF) (left) for global shortwave radiation and (right) for global photosynthetically active radiations.

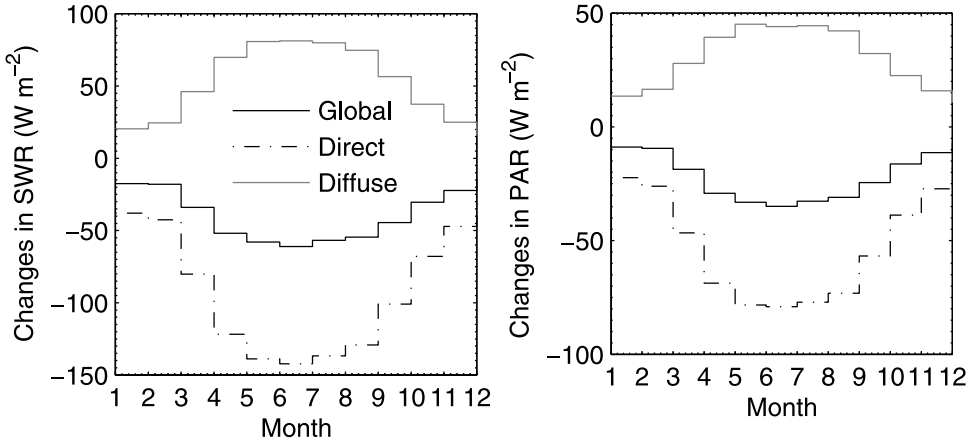

Figure 9. Monthly changes in surface global, direct and diffuse irradiance induced by aerosols for (left) shortwave irradiance and (right) photosynthetically active radiation.

neous quantities. For example, $ADRF_{24hr}$ can be computed as follows:

$$ADRF_{24hr} = (1-\alpha) \times \int_0^{24} (a_1 \times \mu^{a_2}) \times (\exp(a_3 \times \mu^{a_4} \times AOD) - 1)dt/24 \quad (5)$$

where θ can be computed using latitude and Coordinated Universal Time (UTC). Ground-based or satellite measurements of AOD can be used in equation (5) to calculate $ADRF_{24hr}$. Note that the angular dependence of surface albedo is not accounted for, which likely introduces an uncertainty in diurnal mean ADRF of less than 5% [*Yu et al.*, 2004].

[22] Figure 8 (top) presents monthly mean $ADRF_{24hr}$ for SWR and PAR at the surface, respectively. The results were obtained by averaging daily mean $ADRF_{24hr}$ calculated using equation (5) with daily mean AERONET AODs as input. The annual mean ADRF for SWR ($ADRF_{SWR}$) estimated from measurements is -32.8 W m^{-2}, which is very close to that estimated by SBDART simulations (-33.0 W m^{-2}), but larger in magnitude than the estimate of *Li et al.* [2007] (-24.0 W m^{-2}). The discrepancy stems from different background levels used in the analyses. In essence, this study assumes no aerosols in the atmosphere as the reference, whereas the *Li et al.* [2007] method employs a background level of aerosol loading as the reference. The annual mean $ADRF_{SWR}$ decreases to about -24.5 W m^{-2} if the background level of aerosol loading of Li et al. is used in the analysis, which is close to the estimate of *Li et al.* [2007]. $ADRF_{SWR}$ is several factors greater than the average over global land and shows a distinct seasonal variation, namely, -40.2, -48.8, -27.8, and -14.3 W m^{-2} for spring, summer, fall and winter, respectively. The maximum $ADRF_{SWR}$ occurs during summer when both the AOD and the day length reach peak values. The annual mean ADRF for PAR ($ADRF_{PAR}$) derived from PAR-LITE measurements is -22.0 W m^{-2}. $ADRF_{PAR}$ for different seasons is equal to -20.7 W m^{-2} (spring), -25.1 W m^{-2} (summer), -13.7 W m^{-2} (fall), and -6.8 W m^{-2} (winter). These values are about half that for SWR, which is also in good agreement with SBDART simulations.

[23] The normalized ADRF (NADRF, the ratio of ADRF to AOD) indicates the efficiency of the aerosol effect on the surface irradiance (Figure 8, bottom). The annual mean NADRF for the SWR ($NADRF_{SWR}$) derived from measurements and model simulations is -55.2 and -55.7 W m^{-2}, respectively. $NADRF_{SWR}$ shows a moderate seasonal variation, namely, -61.5, -70.2, -49.0, and -39.9 W m^{-2} for spring, summer, fall and winter, respectively. In comparison, the mean $NADRF_{SWR}$ in the Middle East is -85 W m^{-2} [*Markowicz et al.*, 2002] and -75 W m^{-2} over the Indian Ocean [*Ramanathan et al.*, 2001b]. The $NADRF_{SWR}$ is estimated to be -63.9 [*Nakajima et al.*, 2003] and -73 W m^{-2} at Gosan [*Bush and Valero*, 2003]. The overall NADRF of Asian dusts ranges from 65 to 94 W m^{-2} near the east Asian seaboard area [*Kim et al.*, 2005]. In a tropical urban area, the $NADRF_{SWR}$ is about -53 W m^{-2} [*Chou et al.*, 2006]. The $NADRF_{SWR}$ derived in northeastern China during the spring is -48.0 W m^{-2} [*Xia et al.*, 2007]. The difference in the daytime length can contribute significantly to differences in NADRF. Differences in $NADRF_{SWR}$ are also caused by differences in aerosol properties and surface albedo [*Yu et al.*, 2006]. The annual mean NADRF for PAR ($NADRF_{PAR}$) derived from measurements and model simulations is -28.0 and -28.9 W m^{-2}, respectively. A moderate seasonal variation in NADRF is apparent from Figure 8 (bottom right), namely, -32.0, -32.6, -24.4, and -19.2 W m^{-2} for spring, summer, fall and winter, respectively. The value of $NADRF_{PAR}$ during the fall season is close to the value reported by *Xu et al.* [2003] for the Yangtze Delta region in November (-26.3 W m^{-2}).

[24] Aerosols dramatically impact not only global irradiance, but also the partitioning between the direct and diffuse components of surface global irradiance. Figure 9 presents the monthly changes in surface global, direct and diffuse radiation induced by aerosols in the SW and PAR spectra, respectively. The significant reduction in direct radiation due to aerosol scattering and absorption is partly offset by the moderate increase in diffuse radiation. The annual mean changes in global and direct SWR derived from measurements are -38.6 and -89.6 W m^{-2}, respectively. Therefore the mean change in diffuse SWR is 51.0 W m^{-2}. The annual mean changes in global and direct PAR are -21.4 and -51.0 W m^{-2}, respectively, so the annual mean change

in diffuse PAR is 29.6 W m^{-2}. Note that changes in global, direct and diffuse radiation show a distinct seasonal variation with larger values occurring during spring and summer. The ratios of global, direct and diffuse SWR under the condition with aerosol to those without aerosol are about 85%, 63% and 286%; the corresponding ratios for PAR are about 81%, 50% and 350%. This shows that the diffuse fraction of surface irradiance increases dramatically in the presence of aerosols. The increase in diffuse radiation to the surface due to aerosols has two advantages: higher light use efficiency and fewer tendencies to cause canopy photosynthetic saturation [*Roderick et al.*, 2001; *Gu et al.*, 2002]. If the benefit of the increase in diffuse PAR overcomes the loss caused by the decrease in direct PAR for vegetation photosynthetic activities, regional haze in China could enhance crop production. Further studies are required, in which both global irradiance and diffuse irradiance should be considered in assessing the effect of aerosol scattering and absorption on plant growth.

7. Conclusions

[25] Solar broadband and spectral radiation measurements have been made since September 2004 at the Xianghe site, located in a suburban region in northern China. Fifteen months' worth of radiation data are used to explore aerosol effects on surface irradiance. The significant aerosol effects on SWR and PAR are revealed in this paper. Variations in aerosol loading not only change the amount of global solar radiation reaching the Earth's surface but also alter the relative proportions of diffuse and direct surface irradiance.

[26] A parameterization method is developed to describe the relationships between surface irradiance and AOD for different solar zenith angles, which is then used to compute instantaneous and diurnal mean aerosol radiative effects. The estimates of aerosol direct radiative forcing from measurements and from radiative transfer model simulations are in good agreement, with differences generally less than 0.5 W m^{-2}. The annual mean $ADRF_{SWR}$ is -32.8 W m^{-2}. The results show a distinct seasonal variation in $ADRF_{SWR}$, namely, -40.2, -48.8, -27.8, and -14.3 W m^{-2} from spring to winter. The seasonal $ADRF_{PAR}$ is -20.7, -25.1, -13.7, -6.8 W m^{-2} from spring to winter, about half $ADRF_{SWR}$.

[27] Aerosols dramatically impact not only global irradiance, but also the partitioning between direct and diffuse components of surface irradiance. The significant reduction in direct radiation reaching the Earth's surface due to aerosol scattering and absorption is partly offset by the moderate increase in diffuse radiation. The annual mean changes in global and direct SWR derived from measurements are -38.6 and -89.6 W m^{-2}, thus the mean change in diffuse SWR is 51.0 W m^{-2}. The annual mean changes in global and direct PAR are -21.4 and -51.0 W m^{-2}, respectively, so the annual mean change in diffuse PAR is 29.6 W m^{-2}.

[28] **Acknowledgments.** The authors would like to thank the staff at the Xianghe Atmospheric Observatory who oversees a wide range of instruments used in this investigation. The research is partly supported by the National Science Foundation of China (40250120071; 40575058), the Knowledge Innovation Program of the Chinese Academy of Sciences (IAP07115) and the National Basic Research of China (2006CB403702). Z. Li's group is supported by the NASA Radiation Science Program (NNG04GE79G) managed by Hal Maring. We appreciate the comments and suggestions made by three anonymous reviewers that greatly improved the paper.

References

Bush, B. C., and F. P. J. Valero (2003), Surface aerosol radiative forcing at Gosan during the ACE-Asia campaign, *J. Geophys. Res.*, *108*(D23), 8660, doi:10.1029/2002JD003233.

Chameides, W. L., et al. (1999), Case study of the effects of atmospheric aerosols and regional haze on agriculture: An opportunity to enhance crop yields in China through emission controls?, *Proc. Natl. Acad. Sci. U. S. A.*, *96*, 13,626–13,633.

Charlson, R. J., S. E. Schwartz, J. M. Hales, D. Cess, J. A. Coakley, and J. E. Hansen (1992), Climate forcing by anthropogenic aerosols, *Science*, *255*, 423–430.

Che, H. Z., G. Y. Shi, X. Y. Zhang, R. Arimoto, J. Q. Zhao, L. Xu, B. Wang, and Z. H. Chen (2005), Analysis of 40 years of solar radiation data from China, 1961–2000, *Geophys. Res. Lett.*, *32*, L06803, doi:10.1029/2004GL022322.

Cheng, T. T., Y. Liu, D. R. Lu, Y. F. Xu, and H. Y. Li (2006), Aerosol properties and radiative forcing in Hunshan Dake desert, northern China, *Atmos. Environ.*, *40*, 2169–2179.

Chou, M. D., P. H. Lin, P. L. Ma, and H. J. Lin (2006), Effects of aerosols on the surface solar radiation in a tropical urban area, *J. Geophys. Res.*, *111*, D15207, doi:10.1029/2005JD006910.

Conant, W. C. (2000), An observational approach for determining aerosol surface radiative forcing: Results from the first field phase of INDOEX, *J. Geophys. Res.*, *105*, 15,347–15,360.

Dubovik, O., A. Smirnov, B. N. Holben, M. D. King, Y. J. Kaufman, T. F. Eck, and I. Slutsker (2000), Accuracy assessments of aerosol optical properties retrieved from Aerosol Robotic Network (AERONET) Sun and sky radiance measurements, *J. Geophys. Res.*, *105*(D8), 9791–9806.

Dutton, E. G., J. J. Michalsky, T. Stoffel, B. W. Forgan, J. Hickey, D. W. Nelson, T. L. Alberta, and I. Reda (2001), Measurement of broadband diffuse solar irradiance using current commercial instrumentation with a correction for thermal offset errors, *J. Atmos. Oceanic Technol.*, *18*(3), 297–314.

Eck, T. F., B. N. Holben, J. S. Reid, O. Dubovik, A. Smirnov, N. T. O'Neill, I. Slutsker, and S. Kinne (1999), Wavelength dependence of the optical depth of biomass burning, urban and desert dust aerosols, *J. Geophys. Res.*, *104*, 31,333–31,350.

Eck, T. F., et al. (2005), Columnar aerosol optical properties at AERONET sites in central eastern Asia and aerosol transport to the tropical mid-Pacific, *J. Geophys. Res.*, *110*, D06202, doi:10.1029/2004JD005274.

Gu, L., D. Baldocchi, S. B. Verma, T. A. Black, T. Vesala, E. M. Falge, and P. R. Dowty (2002), Advantages of diffuse radiation for terrestrial ecosystem productivity, *J. Geophys. Res.*, *107*(D6), 4050, doi:10.1029/2001JD001242.

Halthore, R. N., et al. (2005), Intercomparison of shortwave radiative transfer codes and measurements, *J. Geophys. Res.*, *110*, D11206, doi:10.1029/2004JD005293.

Holben, B. N., et al. (1998), AERONET—A federated instrument network and data archive for aerosol characterization, *Remote Sens. Environ.*, *66*, 1–16.

Kim, D.-H., B. J. Sohn, T. Nakajima, and T. Takamura (2005), Aerosol radiative forcing over east Asia determined from ground-based solar radiation measurements, *J. Geophys. Res.*, *110*, D10S22, doi:10.1029/2004JD004678.

Li, C. C., et al. (2003), Characteristics of distribution and seasonal variation of aerosol optical depth in eastern China with MODIS products, *Chin. Sci. Bull.*, *48*, 2488–2495.

Li, X. W., and X. J. Zhou (1995), The cooling of Sichuan province in recent 40 years and its probable mechanism, *Acta Meteorol. Sinica*, *9*, 57–68.

Li, Z. (2004), Aerosol and climate: A perspective from east Asia, in *Observation, Theory, and Modeling of the Atmospheric Variability*, pp. 501–525, World Sci., Hackensack, N. J.

Li, Z., and A. Trishchenko (2001), Quantifying the uncertainties in determining SW cloud radiative forcing and cloud absorption due to variability in atmospheric condition, *J. Atmos. Sci.*, *58*, 376–389.

Li, Z., et al. (2007), Remote sensing of aerosol optical properties and its radiative effects in Northern China, *J. Geophys. Res.*, doi:10.1029/2006JD007382, in press.

Liang, F., and X. Xia (2005), Long-term trends in solar radiation and the associated climatic factors over China for 1961–2000, *Ann. Geophys.*, *23*, 2425–2432.

Long, C. N., and T. P. Ackerman (2000), Identification of clear skies from broadband pyranometer measurements and calculation of downwelling shortwave cloud effects, *J. Geophys. Res.*, *105*, 15,609–15,626.

Luo, Y., D. Lu, X. Zhou, W. Li, and Q. He (2001), Characteristics of the spatial distribution and yearly variation of aerosol optical depth over China in last 30 years, *J. Geophys. Res.*, *106*(D13), 14,501–14,513.

Mao, J., and C. Li (2005), Observation study on aerosol radiative properties over China (in Chinese), *Acta Meteorol. Sinica*, *63*, 622–635.

Markowicz, K. M., P. J. Flatau, M. V. Ramana, P. J. Crutzen, and V. Ramanathan (2002), Absorbing mediterranean aerosols lead to a large reduction in the solar radiation at the surface, *Geophys. Res. Lett.*, *29*(20), 1968, doi:10.1029/2002GL015767.

Michalsky, J., E. Dutton, D. Nelson, M. Rubes, T. Stoffel, M. Wesley, M. Splitt, and J. DeLuisi (1999), Optimal measurement of surface shortwave irradiance using current instrumentation, *J. Atmos. Oceanic Technol.*, *16*, 55–69.

Michalsky, J. J., et al. (2005), Toward the development of a diffuse horizontal shortwave irradiance working standard, *J. Geophys. Res.*, *110*, D06107, doi:10.1029/2004JD005265.

Nakajima, T., et al. (2003), Significance of direct and indirect radiative forcings of aerosols in the East China Sea region, *J. Geophys. Res.*, *108*(D23), 8658, doi:10.1029/2002JD003261.

Ohmura, A., et al. (1998), Baseline Surface Radiation Network (BSRN/WCRP): New precision radiometry for climate research, *Bull. Am. Meteorol. Soc.*, *79*, 2115–2136.

Philipona, R. (2002), Underestimation of solar global and diffuse radiation measured at Earth's surface, *J. Geophys. Res.*, *107*(D22), 4654, doi:10.1029/2002JD002396.

Qian, Y., D. P. Kaiser, L. R. Leung, and M. Xu (2006), More frequent cloud-free sky and less surface solar radiation in China from 1955 to 2000, *Geophys. Res. Lett.*, *33*, L01812, doi:10.1029/2005GL024586.

Ramanathan, V., P. J. Crutzen, J. T. Kiehl, and D. Rosenfeld (2001a), Aerosols, climate, and the hydrological cycle, *Science*, *294*, 2119–2124.

Ramanathan, V., et al. (2001b), Indian Ocean Experiment: An integrated analysis of the climate forcing and effects of the great Indo-Asian haze, *J. Geophys. Res.*, *106*, 28,371–28,398.

Ricchiazzi, P., S. Yang, C. Gautier, and D. Sowle (1998), SBDART: A research and teaching software tool for plane-parallel radiative transfer in the Earth's atmosphere, *Bull. Am. Meteorol. Soc.*, *79*, 2101–2114.

Roderick, M. L., G. D. Farquhar, S. L. Berry, and I. R. Noble (2001), On the direct effect of clouds and atmospheric particles on the productivity and structure of vegetation, *Oecologia*, *129*(1), 21–30, doi:10.1007/s004420100760.

Ross, J., and F. M. Sulev (2000), Sources of errors in measurements of PAR, *Agric. For. Meteorol.*, *100*, 103–125.

Satheesh, S. K., and V. Ramanathan (2000), Large differences in tropical aerosol forcing at the top of the atmosphere and Earth's surface, *Nature*, *405*, 60–63.

Schaaf, C. B., et al. (2002), First operational BRDF, albedo and nadir reflectance products from MODIS, *Remote Sens. Environ.*, *83*, 135–148.

Smirnov, A., B. N. Holben, T. F. Eck, O. Dubovik, and I. Slutsker (2000), Cloud screening and quality control algorithms for the AERONET database, *Remote Sens. Environ.*, *73*, 337–349.

Stoffel, T. (2005), Solar Infrared Radiation Station handbook, *ARM Tech. Rep. ARM-TR-035*, Natl. Renewable Energy Lab., Golden, Colo. (Available at http://www.arm.gov)

Wang, H., G. Y. Shi, B. Wang, and T. L. Zhao (2004), Radiative forcing due to dust aerosol over east Asia-north Pacific region during spring 2001, *Chin. Sci. Bull.*, *20*, 2212–2219.

Wang, M. X., R. J. Zhang, and Y. F. Pu (2001), Recent researches on aerosol in China, *Adv. Atmos. Sci.*, *18*, 576–586.

Xia, X., H. B. Chen, P. C. Wang, X. M. Zong, and P. Gouloub (2005), Aerosol properties and their spatial and temporal variations over north China in spring 2001, *Tellus, Ser. B*, *57*, 28–39.

Xia, X., et al. (2006), Variation of column-integrated aerosol properties in a Chinese urban region, *J. Geophys. Res.*, *111*, D05204, doi:10.1029/2005JD006203.

Xia, X., H. Chen, Z. Li, P. Wang, and J. Wang (2007), Significant reduction of surface solar irradiance induced by aerosols in a suburban region in northeastern China, *J. Geophys. Res.*, *112*, D22S02, doi:10.1029/2006JD007562.

Xu, J., M. H. Bergin, R. Greenwald, and P. B. Russell (2003), Direct aerosol radiative forcing in the Yangtze delta region of China: Observation and model estimation, *J. Geophys. Res.*, *108*(D2), 4060, doi:10.1029/2002JD002550.

Xu, Q. (2001), Abrupt change of the midsummer climate in central east China by the influence of atmospheric pollution, *Atmos. Environ.*, *35*, 5029–5040.

Yu, H., et al. (2004), The Direct radiative effect of aerosols as determined from a combination of MODIS retrievals and GOCART simulations, *J. Geophys. Res.*, *109*, D03206, doi:10.1029/2003JD003914.

Yu, H., et al. (2006), A review of measurement-based assessments of the aerosol direct radiative effect and forcing, *Atmos. Chem. Phys.*, *6*, 613–666.

Zong, X. M., J. H. Qiu, and P. C. Wang (2005), Characteristics of atmospheric aerosol optical depth over 16 radiation stations in the last 10 years (in Chinese), *Clim. Environ. Res.*, *10*, 201–208.

H. Chen, P. Wang, and X. Xia, Institute of Atmospheric Physics, Chinese Academy of Sciences, Beijing 100021, China. (xiaxiangao2000@yahoo.com)

M. Cribb and Z. Li, Department of Atmospheric and Oceanic Science and Earth System Science Interdisciplinary Center, University of Maryland, College Park, MD 20742, USA.